CLASSIFICATION OF CLOUDY HYPERSPECTRAL IMAGE AND LIDAR DATA BASED ON FEATURE FUSION AND DECISION FUSION

Renbo Luo[1,2], *Wenzhi Liao*[1], *Hongyan Zhang*[1,3], *Youguo Pi*[2], *Wilfried Philips*[1]

[1]Ghent University-TELIN-IPI-iMinds, Gent, Belgium
[2]School of Automation Science and Engineering, South China University of Technology, China
[3]State Key Lab. of Inf. Eng. in Surveying, Mapping and Remote Sensing, Wuhan University, China

ABSTRACT

Hyperspectral and LiDAR data, can provide plentiful information about the objects on the Earths surface. However there are some shortages for each of them, where hyperspectral sensor is easily influenced by cloud and difficult to distinguish different objects contained same materials, LiDAR cannot discriminate different objects which are similar in altitude. Fusion of these multi-source data for reliable classification attracts increasing interests but remains challenging. In this paper, we propose a new framework to fuse multi-source data for classification. The proposed method contains three main works: 1) cloud shadows extraction; 2) feature fusion of spectral and spatial information extracted from hyperspectral image, elevation information extracted from LiDAR data; 3) decision fusion of cloud and non-cloud regions. Experimental results on real HSI and LiDAR data demonstrate effectiveness of the proposed method both visually and quantitatively.

Index Terms— Remote sensing, feature fusion, hyperspectral image, LiDAR data

1. INTRODUCTION

Recently advanced sensor technologies allow us to measure different aspects of the objects on the Earths surface, from spectral characteristics in hyperspectral images (HSI), to height information in Light Detection And Ranging (LiDAR) data. HSI can provide valuable information of different objects of interest, but cannot distinguish different objects made of the same material, and it is easily influenced by cloud. LiDAR data provides useful information related to the size, structure and elevation of different objects, but difficult to discriminate different objects which are similar in altitude but quite different in nature. Using single data source (either HSI or LiDAR data) might not be sufficient to obtain reliable classification results in a complex urban context. These multi-source data, once combining, can contribute to a more comprehensive interpretation of the ground objects [1]- [3].

This work was supported by China Scholarship Council and the FWO project G037115N: Data fusion for image analysis in remote sensing.

To model the spatial information, attribute profiles (APs) [4] provide a multilevel characterization of an image by the sequential application of morphological attribute filters. In [5], extended multi-attribute profiles (EMAPs) are taken into account in order to extract abundant spatial information in hyperspectral images and it makes an obviously contribution for the classification. In [6], the method applied morphological attribute profiles (EAPs) [7] to both HSI and LiDAR data for a classification task, it stacked spectral features, spatial and elevation features (extracted by EAPs) directly. However, stacking high dimensional HSI and features extracted by EMAPs directly may leads to the problem of the curse of dimensionality and excessive computation time. Furthermore, there exists cloud shadows in some HSI, the spectral information of samples under cloud shadows are completely different from normal samples, thus has negative influence on the application of classification.

In this paper, we propose a framework to classify the objects under cloud shadows by feature fusion and decision fusion of hyperspectral image and LiDAR data. The proposed method first extracts the cloud shadows as a mask for the step of decision fusion, as well as to better make use of the advantages of HSI and LiDAR data. Instead of stacking the high dimensional HSI, EMAPs computed on HSI and EMAPs computed on LiDAR data directly, we reduce their dimensionality first by feature extraction method, and then fuse the extracted low dimensional spectral, spatial and elevation features in a stacked architecture for classification. In order to extract spatial and elevation information, we used EMAPs with four attributes: area, length of diagonal of the bounding box, moment of inertia and standard deviation. What's more, we used recently proposed Rotation Forest (RoF) [8] as a classifier in proposed method.

2. PROPOSED FRAMEWORK

In this section, we detail our proposed method, Fig. 1 shows the proposed framework, feature extraction (FE) method is first performed on HSI and extracted low dimensional spectral features (Fspe). In parallel, the HS data are transformed

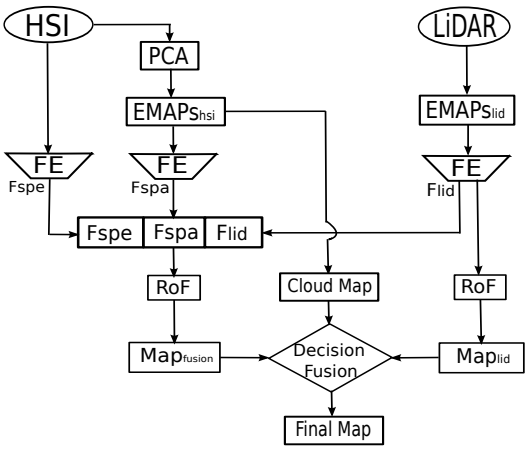

Fig. 1: Flowchart of the proposed framework

by principal component analysis (PCA), and the first few important principal components (PCs) are used as base images for EMAPs, producing EMAPs$_{hsi}$. Then FE is performed on the high dimensional EMAPs$_{hsi}$ to extracted low dimensional spatial features (Fspa). At the same time, the cloud map can be extracted by using EMAPs$_{hsi}$. The elevation features (Flid) are extracted from EMAPs$_{lid}$ (EMAPs computed on LiDAR data). After fusing Fspe, Fspa and Flid on feature level, we use the fused features and Flid as input of RoF [8] classifier independently to generate two classification maps (Map$_{fusion}$ and Map$_{lid}$). The final classification map can be obtained by decision fusion of those two classification maps based on the cloud map Fig. 2b. In the following, the individual parts of the proposed framework will be discussed in details.

2.1. Cloud shadows mask Extracted

Attribute Profiles (APs) are a multi-level decomposition of the input image based on attribute filters. For area attribute profiles, it can remove the objects that smaller than the given attribute values, and as the size of cloud-covered regions is much larger than the objects on the Earths surface, if the given attribute values is bigger than the objects on the ground and smaller than the size of cloud-covered regions, we can extract the cloud shadows through the area attribute filters. Based on this idea, from the cloudy HSI [9], we extract the cloud shadows (cloud map) as Fig. 2b. Let $\mathbf{G} = \{g_{ij}\}$ denote the cloud shadows mask, for the cloud shadows regions, the value of pixel $g_{ij} = 0$; for the other regions, $g_{ij} = 1$.

2.2. Feature Fusion

As indicated in Fig. 1, the original HSI are transformed by feature extraction (FE) approach in order to get a few effective features (Fspe). In parallel, the HSI are transformed by PCA, and the first few important PCs that correspond to 99% of the cumulative variance are used as based images

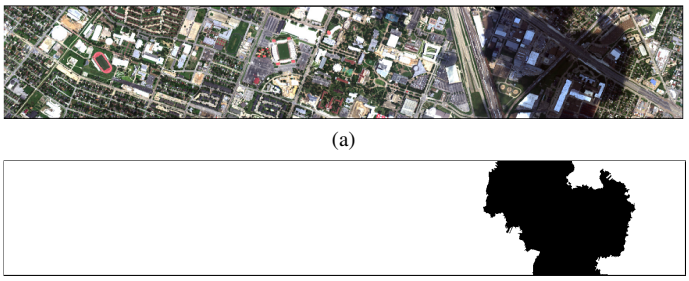

(a)

(b)

Fig. 2: a)False RGB image of HS data; (b) Extracted Cloud-covered map

for EMAPs. Suppose each AP is composed of n thickening and n thinning transformations of the corresponding PC for each attribute, and the number of attributes is m, we come up with $m \times (2n) + 1$ number of features in each EAP. Finally, the number of features in the EMAPs by considering c PCs is equal to $c \times (m \times (2n) + 1)$. If we choose many values for each attribute, as n is big, then the number of features in the EMAPs is very large. In order to reduce redundancy, avoid curse of dimensionality and speed up processing time in classification, we extract few effective spatial features (Fspa) from EMAPs$_{hsi}$, and few effective elevation features (Flid) from EMAPs$_{lid}$. Last but not least the low dimensional Fspe, Fspa and Flid are concatenated into one stacked vector to form fused features (Ffusion).

2.3. Decision Fusion

After fusing spectral, spatial and elevation features on feature level, we use the fused features Ffusion as input of RoF to generate 'Map$_{fusion}$' $\mathbf{A} = \{a_{ij}\}$, and use only elevation features Fspe as input of RoF to generate 'Map$_{lid}$' $\mathbf{B} = \{b_{ij}\}$. The final classification map $\mathbf{F} = \{f_{ij}\}$ is provided by fusing those two classification maps based on non-cloud and cloud maps, as:

$$f_{ij} = g_{ij} \times a_{ij} + (1 - g_{ij}) \times b_{ij} \quad (1)$$

This means the proposed method exploit the different contributions of those two classification maps, 'Map$_{lid}$' makes contribution to the cloud-covered regions in the final map, as the information from LiDAR data is not influenced by cloud; 'Map$_{fusion}$' makes contribution to the other regions, as it make best use of spatial, spectral and elevation features.

3. EXPERIMENTAL RESULTS

The data set in our experiments were captured by the NSF-funded Center on June 2012 over the University of Houston campus and the neighboring urban area. This data set consists of a HSI and a LiDAR derived DSM, both at the same spatial resolution (2.5m). The HSI has 144 spectral bands with a wavelength range from 380 to 1050 nm, with 349×1905

pixels, contains 15 classes. Available training and testing sets are given in Table 1 (number of training samples/ number of test samples), the false color image of this data set is shown on Fig. 2, for more information, see [9].

The input HSI is transformed by PCA, and the first two PCs with a cumulative variation of more than 99% are kept. We choose PCA, which is simple and fast, as feature extraction method, and apply Rotation Forest (RoF) [8] classifier in our experiments. Our proposed method is compared with the following schemes: 1) using the original HSI (Raw$_{hsi}$); 2) using features extracted from original HSI (Fspe); 3) using features extracted from EMAPs$_{hsi}$(Fspa); 4) using features extracted from EMAPs$_{lid}$ (Flid) ; 5) using features extracted from the vector by stacking original HSI, EMAPs$_{hsi}$ and EMAPs$_{lid}$ (FEstacked); 6) using fused features which stacking Fspe, Fspa and Flid (Ffusion). The classification results are quantitatively evaluated by measuring the overall accuracy (OA), the average accuracy (AA), Kappa coefficient (κ) on the test samples. Table 1 shows the accuracies values obtained from the experiments, Fig. 3 shows the classification maps.

Based on our experimental results, the proposed method has better results in terms of OA, AA, κ and the classification map. In particular, the improvements of proposed method in OA are 2%-11.6% compared to the schemes of others. It also can be found that using only spectral feature is not sufficient for a reliable classification, fusion of the spectral features, the spatial and the elevation features which extracted from EMAPs features can improve the classification performances. By comparing the results reported in Tables 1, it is easy to infer that fusing the features extracted from each source (HSI, EMAPs$_{hsi}$ and EMAPs$_{lid}$) works better than using the features extracted from a stacked vector which have stacked original HSI, EMAPs$_{hsi}$ and EMAPs$_{lid}$. The main reason may be closely related to the fact that features from different source have different nature, if we stacked them first, and then reduce their high dimensionality together, some important information would be lost or mixed, thus cannot make full use of the advantages of each feature source.

By comparing the classification maps, we can see visually that the objects under cloud regions are not well classified by using the information from HSI. The cloud-covered regions are classified well by using features extracted from LiDAR data, because the elevation information contained in EMAPs$_{lid}$ is not influenced by cloud. When stacking all feature sources together, the no cloud-covered regions are classified well. The proposed method combines the advantages of these two schemes, leads to classification maps with higher quality.

4. CONCLUSION

The contribution of this paper is the definition of a framework for cloudy HSI and LiDAR data classification based on feature fusion and decision fusion, by combining characterization of spectral, spatial and elevation information. In greater detail, our proposed method extracts the cloud shadows first as a mask for the fusion of two classification maps. The first classification map is generated from fused features, which fuse the spectral and spatial features from HSI and elevation features from LiDAR data, the second classification map comes from the RoF classifier which only use elevation features as an input. After the decision fusion, we get a final classification map with high quality. Experimental results on the classification of the real HSI and LiDAR data show the efficiency of the proposed framework, it can combine the advantages of hyperspectral data and LiDAR data, and makes them complement each other well. In addition, the proposed approach can be thought of as a general framework, the feature extraction method can be replaced by other techniques (supervised or semi-supervised feature extraction), possibly to improve classification accuracy. In future work, we will validate the proposed method by extending it to more data sets.

Acknowledgment

The authors would like to thank the Hyperspectral Image Analysis group and the NSF Funded Center for Airborne Laser Mapping (NCALM) at the University of Houston for providing the data sets used in this study.

5. REFERENCES

[1] M. Dalponte, L. Bruzzone and D. Gianelle, "Fusion of hyperspectral and LIDAR remote sensing data for classification of complex forest areas," *IEEE Trans. Geosci. Remote Sens.*, vol. 46, no. 5, pp. 1416-1427,2008.

[2] W. Liao, A. Pižurica, R. Bellens, S. Gautama and W. Philips, "Generalized Graph-Based Fusion of Hyperspectral and LiDAR Data Using Morphological Features," *IEEE Geosci. Remote Sens. Lett.* , vol. 12, no. 3, pp. 552-556, Mar. 2015.

[3] W. Liao, R. Bellens, A. Pižurica, S. Gautama and W. Philips, "Combining Feature Fusion and Decision Fusion for Classification of Hyperspectral and LiDAR Data," *In Proc. IEEE IGARSS,* , Quebec City, QC , Jul. 13-18 , vol. 1, pp. 1241-1244, 2014.

[4] M. Dalla Mura, J. Benediktsson, B. Waske, and L. Bruzzone, "Morphological attribute profiles for the analysis of very high resolution images," *IEEE Trans. Geosci. Remote Sens.*, vol.48, no.10, pp. 3747-3762, 2010.

[5] M. Dalla Mura, A. Villa, J. A. Benediktsson, J. Chanussot, L. Bruzzone, "Classification of Hyperspectral Images by Using Extended Morphological Attribute Profiles and Independent Component Analysis," *IEEE Geosci. Remote Sens. Lett.*, Vol. 8, No. 3, pp. 541-545, May 2011.

Table 1: Classification accuracies obtained by the described schemes.

	Raw_{hsi}	Fspe	Fspa	Flid	FEstacked	Ffusion	Proposed
Number of Features	144	15	15	15	45	45	-
Grass Healthy (198/1053)	82.18	82.24	83.19	58.40	83.27	**83.47**	**83.47**
Grass Stressed (190/1064)	82.52	82.71	76.69	61.37	83.83	84.16	**84.21**
Grass Synthetis (192/505)	99.80	**100**	**100**	94.85	**100**	**100**	**100**
Tree (188/1056)	93.37	89.67	83.95	76.70	92.88	91.75	**98.58**
Soil (186/1056)	97.92	98.58	98.30	83.14	99.43	**99.81**	**99.81**
Water (182/143)	95.10	**99.30**	84.62	95.80	95.10	95.80	95.80
Residential (196/1072)	76.76	79.27	84.15	83.12	85.71	**97.58**	96.96
Commercial (191/1053)	55.36	49.38	37.97	93.44	83.76	75.59	**94.30**
Road (193/1059)	78.47	75.82	79.61	66.95	85.71	92.82	**94.15**
Highway (191/1036)	59.82	**80.78**	66.31	70.64	70.85	75.87	74.89
Railway (181/1054)	79.51	88.14	77.71	96.86	97.25	**99.35**	98.76
Parking Lot 1 (192/1041)	84.34	78.19	88.18	66.38	89.15	**97.69**	**97.69**
Parking Lot 2 (184/285)	72.28	71.58	72.63	63.86	**80.00**	77.89	77.89
Tennis Court (181/247)	99.60	99.60	**100**	99.60	**100**	**100**	**100**
Running Track (187/473)	97.67	97.46	**100**	58.77	98.94	98.73	99.15
OA (%)	81.02	82.14	79.95	76.15	88.38	90.81	**92.82**
AA (%)	83.61	84.54	83.26	77.16	89.35	91.35	**92.97**
κ	0.799	0.815	0.785	0.748	0.879	0.903	**0.921**

(a) (b) (c) (d) (e) (f) (g)

Fig. 3: Classification maps produced by the described schemes. (a) Raw_{hsi} (b) Fspe; (c) Fspa; (d) Flid; (e) FEstacked; (f) Ffusion ; (g) Proposed

[6] M. Pedergnana, P. Reddy Marpu, M. Dalla Mura, J. A. Benediktsson, L. Bruzzone, "Classification of Remote Sensing Optical and LiDAR Data Using Extended Attribute Profiles," *IEEE Journals on Selected Topics in Signal Processing*, vol. 6, no. 7, pp. 856-865, Nov. 2012.

[7] M. Dalla Mura, J. A. Benediktsson, B. Waske, and L. Bruzzone, "Extended profiles with morphological attribute filters for the analysis of hyperspectral data," *Int. J. Remote Sens.*, vol. 31, no. 22, pp. 5975-5991, Nov. 2010.

[8] J. Xia, P. Du, X. He, and J. Chanussot, "Hyperspectral remote sensingimage classification based on rotation forest," *IEEE Geosci. Remote Sens. Lett.*, vol. 11, no. 1, pp. 239-243, Jan. 2014.

[9] 2013 IEEE GRSS Data Fusion Contest, Online: *http://www.grss-ieee.org/community/technical-committees/data-fusion/*.